Resistance performance of a ship in brash ice channel using CFD and DEM coupling model

Xie Chang[1,2], Lu Mingfeng[1], Zhou Li [2*], Zhou Xu[1]

(1. Nantong COSCO KHI Ship Engineering Co., Ltd., Nantong, 226001; 2. Jiangsu University of Science and Technology, Zhenjiang, 212003)

Abstract： The brash ice channel formed with icebreaker navigation is a normal working scenario for ice-going vessels. Therefore, it is necessary to study the brash ice resistance in this condition. In this paper, CFD and DEM coupling method was adopted to investigate the resistance performance of a ship sailing in model-scaled brash ice fields, considering the collision force and friction resistance among the brash ice, the water resistance, and the hydrodynamic force of brash ice, which make up the physical scenarios of navigation in the brash ice channel. Firstly, the resistance in brash ice channel was simulated by using CFD and DEM coupling methods. Then, the numerical simulation results were compared with the experimental results in HSVA ice tank. It was shown that the error between the numerical simulation results and the test results is less than 5%, which shows the robustness of the present coupling strategy. And the movement of broken ice is consistent with the experimental phenomenon

Keywords: Discrete element method; CFD and DEM coupling; Numerical simulation; Brash ice resistance.

1. Introduction

With the Arctic route becoming more available, the number of ships navigating the Arctic route is increasing. Icebreakers are needed to navigate the Arctic route for ships of low ice class，to form a brash ice channel. Therefore, it is significant to study the channel resistance of brash ice. The brash ice channel is characterized by the ice-water mixed multiphase flow. The resistance is usually evaluated by the empirical formula method, numerical simulation method, and ship model test method.

The most acceptable empirical formula method is the Finnish-Swedish Ice Class Rules (FSICR) based on the Baltic Sea ice conditions (Trafi, 2010, 2011), and most classification societies use the FSICR assessment method. However, the brash ice resistance predicted by FSICR is usually higher than that of the ice tank test (Cho et al., 2013; Zhang et al., 2013). To extend the FSICR brash ice channel resistance assessment method to the Arctic, Karulina et al. proposed a computational model based on the FSICR method to estimate the ice resistance of ice-broken channels considering the special environment of the Arctic. There were still many factors not considered in the severe and moderate ice conditions (Karulina et al., 2019). Dobrodeev et al. established a theoretical model to calculate the resistance of the brash ice channel based on the real ship data and test data. The theoretical model was in good agreement with the ice tank test results (Dobrodeev et al., 2019).

The ship model test is the most acceptable method to evaluate the brash ice resistance, which can be divided into the refrigerated ice test in ice tank and synthetic ice test in the conventional towing tank. The ice tank test is the closest method to the actual ice condition, but its cost is high. Cho et al. carried out a brash ice resistance test in a square ice tank at the Korea Research Institute of the Ship and Ocean Engineering (KRISO) (Cho et al., 2013). Jeong et al. conducted a brash ice channel resistance test based on the Finnish Transport Safety Agency (2017) and Swedish Transport Agency (2011) in the KRISO ice tank. The IA ice class and IB ice class brash ice resistance test were carried out in the ice tank, and the model test results were compared with the results of FSICR formula (Jeong et al., 2017). In 2019, the effects of channel width, ice concentration, and ice thickness on the brash ice resistance in the ice tank were studied (Jeong et al., 2019). Zhou et al. carried out a brash ice test at the Aalto University Ice Tank in Finland to study the effects of ice thickness, speed and heading angle on the resistance (Zhou et al., 2019).

For scientific research institutes without ice tank test, the synthetic ice in the conventional towing tank is alternative. Kim et al. carried out the brash ice resistance test in towing tank and compared the results with the brash ice resistance test in an ice tank (Kim et al., 2019). Guo et al. carried out the experimental study on the resistance in the brash ice channel by using the synthetic ice and studied the resistance characteristics under the conditions of four concentrations (Guo et al., 2018). Luo et al. used the synthetic ice to investigate the interaction of ship-wave-ice in the periglacial area, and the effect of wavelength, wave height and ice concentration on the additional coupling resistance (Luo et al., 2018). Zong et al. also used synthetic ice to study the effect of different ice shape, ice concentrations and speed of brash ice on the resistance of brash ice (Zong et al., 2020).

The ice–ship interaction modeling using numerical methods has been shown to be both efficient and accurate. The main numerical simulation methods are finite element method (FEM) and discrete element method (DEM). Kim et al. simulated brash ice resistance of 60%~90% ice concentrations using LS-DYNA software, and the results were compared with synthetic ice test (Kim et al., 2013, 2014). Guo and Wang also used LS-DYNA to simulate the brash ice resistance and compared with the results of synthetic ice test (Guo et al., 2018; Wang et al., 2020). Yang et al. based on LS-DYNA brash ice resistance test simulation and compared with DuBrovin empirical formula (Yang et al., 2020). Kim et al. investigated brash ice resistance with ABAQUS, and compared the results with ice tank test results (Kim et al., 2019). However, the finite element method cannot simulate the water resistance of the ship which play an important role in the real brash ice channel, also with expensive calculation cost, there are few studies on the simulation of brash ice channel resistance by finite element method. As for the discrete element method, Ji et al. used DEM to construct three-dimensional disk-shaped brash ice to simulate the interaction between ship and ice (Ji et al., 2013). Van den Berg et al. studied the influence of floating ice shape on the ice load of vertical structures based on DEM (Van den Berg et al., 2019). Based on the DEM method of STAR CCM+ software, Luo et al. studied the simulation of brash ice channel resistance of a bulk carrier and compared it with the ice tank test results (Luo et al., 2020). Guo et al. based on STAR CCM+ software with DEM method to study the resistance performance of a ship in ice field with different ice concentrations and compared with the results of synthetic model ice test (Guo et al., 2020). Huang et al. also used the DEM method based on STAR CCM + software and compared it with the results of Guo’s synthetic model ice test (Huang et al., 2020). Polojärvi et al. used self-developed DEM method to simulate the resistance performance of an actual ship in the floating ice field, and the simulation results were in good agreement with the actual ship navigation data (Polojärvi et al., 2021). Yang et al. used self-developed DEM method to simulate the brash ice resistance, and the effects of the brash ice shape, the brash ice concentration, and the friction coefficient of ship-ice on the brash ice resistance were studied by using DEM (Yang et al., 2021).

Following icebreaker navigation, the size of the brash ice in the brash ice channel is small, and the possibility of the second break is low, so we can assume that the brash ice resistance caused by the second break can be ignored. Therefore, the resistance of polar ship in the brash ice channel mainly includes brash ice resistance and water resistance. The resistance of brash ice is mainly caused by the collision of ship-ice and the friction of ship-ice. The brash ice is affected by the viscosity of water by the hull movement, and the water resistance on both the ice and the hull cannot be ignored. Therefore, it is practical to use viscous CFD and DEM coupling to evaluate the resistance of the brash ice channel. In this paper, the coupling method of CFD and DEM with STAR CCM+ software was used to analyze the influence of numerical simulation parameters. The numerical simulation configuration is present, and the influence of parameters on the movement of brash ice was investigated.

2 Basic formulation of numerical model

In the numerical model, the fluid is an incompressible Newtonian fluid that satisfies the continuity equation and the momentum conservation equation, ignoring the heat exchange between the fluid and the discrete ice. For the brash ice, the Lagrangian DEM method was adopted.

2.1 CFD numerical model

The motion of an incompressible Newton fluid satisfies the continuity equation and conservation of momentum equations:

$$\frac{\partial(u_i)}{\partial x_i}=0 \tag{1}$$

$$\frac{\partial u_i}{\partial t}+\frac{\partial u_i u_j}{\partial x_j}=\frac{\partial}{\partial x_j}(\mu\frac{\partial u_i}{\partial x_j})-\frac{1}{\rho}\frac{\partial p}{\partial x_i}+S_j \tag{2}$$

where u_i and u_j are the time mean of the velocity component (i, j = 1,2,3), P is the time mean of the pressure, ρ is the fluid density, μ is the dynamic viscosity coefficient, S_j is the generalized source term of the momentum equation.

The governing equations are solved by the coupling of pressure, in which the convection term is discretized by the second-order upwind scheme and the dissipation term is discretized by the second-order central difference scheme. Considering the effect of Wall Shear Force on the model, the SST (Shear Stress Transport) k-ω model was adopted in order to simulate the strong counter-pressure gradient flow, and the reference (Menter, 1994) shows specific equations.

2.2 DEM particle contact model

2.2.1 The contact model of particle-particle and particle-wall

In the simulation process, the contact and collision between particles and between particles and walls is the inevitable result of particle motion. Therefore, in terms of contact stress, this paper chooses a computationally efficient and accurate linear spring contact model, which is a contact model based on the results of Coudall and Strack (Cundall et al., 1979). The contact force model is shown in Figure 1. F_n is the normal force and F_t is the tangential force.

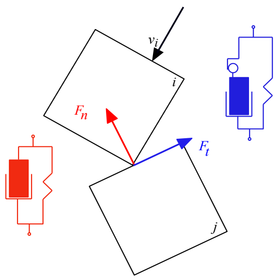

Fig. 1 Spring-damper contact force model

The contact force between two particles is:

$$F_{contact}=F_{nij}+F_{tij} \tag{3}$$

where F_{nij} is the normal force and F_{tij} is the tangential force.

The normal force is:

$$F_n=-K_n d_n-N_n v_n \tag{4}$$

where K_n is the normal spring stiffness; d_n is the normal overlap of the contact point, N_n is the normal damping, and v_n is the normal component of the sphere surface velocity at the contact point.

The expression for the tangential force is:

$$F_n = \begin{cases} -K_t d_t - N_t v_t, & \left|K_t d_t\right| < \left|K_n d_n\right| C_{fs} \\ \dfrac{\left|K_n d_n\right| C_{fs} d_t}{\left|d_t\right|}, & \left|K_t d_t\right| > \left|K_n d_n\right| C_{fs} \end{cases} \qquad (5)$$

where K_t is the tangential spring stiffness; d_t is the tangential overlap of the contact point, N_t is the tangential damping, v_t is the tangential component of the sphere surface velocity at the contact point, and C_{fs} is the friction coefficient between particles.

2.2.2 The interaction model of particle-fluid

The interaction of DEM particle in the flow field mainly includes the buoyancy of the particle, the resistance of the flow field to the particle, the additional mass force and the lift force on the particle. This paper mainly calculates drag resistance, additional mass force and pressure gradient force (including buoyancy effect). In the coupled calculation process, the moving DEM particles are subject to drag resistance due to the existence of fluid viscosity, and the drag resistance of the particles is usually solved by the resistance coefficient. The solution of the DEM particle resistance coefficient in this paper is achieved by the Haider and Levenspiel resistance coefficient (Haider et al., 1989).

The drag resistance on the particle:

$$F_d = \frac{1}{2} C_d \rho A_p \left|v_s\right| v_s \qquad (6)$$

where C_d is the particle resistance coefficient, ρ is the fluid density, v_s is the particle slip velocity (v_s=v_c-v_d), v_c is the water velocity, and v_d is the particle velocity.

The additional mass force on the particle:

$$F_a = C_{vm} \rho V_p \left(\frac{Dv_s}{D_t} - \frac{dv_p}{d_t} \right) \qquad (7)$$

where C_{vm} is the additional mass coefficient of the particle, V_p is the particle volume, ρ is the fluid density, and v_p is the absolute velocity of the particle.

DEM particles are subjected to pressure gradient force in addition to fluid resistance and additional mass force. The expression of pressure gradient force on the particle:

$$F_p = -V_p \nabla p_{static} \qquad (8)$$

where V_p is the volume of particles and ∇p_{static} is the gradient of static pressure in continuous.

2.3 CFD-DEM coupled numerical model

The motion of incompressible Newtonian fluid satisfies continuity equation and momentum conservation equation (Norouzi et al., 2016).

$$\frac{\partial(\rho_f \varepsilon_f)}{\partial t} + \nabla \cdot (\rho_f \varepsilon_f \vec{u}) = 0 \qquad (9)$$

$$\frac{\partial(\rho_f \varepsilon_f \vec{u})}{\partial t} + \nabla \cdot (\rho_f \varepsilon_f \vec{u} \cdot \vec{u}) = -\varepsilon_f \nabla p - \nabla \cdot (\varepsilon_f \vec{\tau}_f) + \rho_f \varepsilon_f \vec{g} - \vec{F} \qquad (10)$$

where ρ_f is the density of fluid term; ε_f is the volume fraction of the fluid term in the control volume; $\bar{u}$ is the average velocity of fluid; p is the mean value of pressure; $\vec{F}$ is the volume average of the resistance of particles to the surrounding fluid in the discrete ice term of the control volume, including resistance, pressure gradient force, shear stress, and so on.

3. The configuration of numerical simulation

3.1 Research object

The research object of this paper was the ice-strengthened Panamax bulk carrier. The model test was carried out in HSVA ice tank. The test items were the FSICR IA ice class and IB ice class brash ice channel test. The scale of the ship model was consistent with that of the Hamburg ice tank, and the scale ratio was 30.682, as shown in Figure 2. The main parameters of the ship model are shown in Table 1.

Fig. 2 The geometric ship model

Table 1 Main parameters of the ship model

Parameters	Full ship	Ship model
Scale ratio λ	1	30.682
Length between perpendiculars L_{pp}(m)	217.00	7.073
Waterline length L_{wl}(m)	221.07	7.205
Ship breath B (m)	32.25	1.051
Draft T (m)	14.73	0.480
Ship speed V (m/s)	5.00	0.464
Fourier number Fr	0.0557	0.0557

3.2 Numerical simulation setup

A full ship model was used in the numerical simulation since the asymmetric brash force on the ship. In accordance with the HSVA ice tank test conditions, the width of the brash ice channel was 2 times the ship breath, the calculated domain size of the brash ice channel was $-2.5\ L_{pp} \leq x \leq 3\ L_{pp}$, $-2.0\ L_{pp} \leq y \leq 2.0\ L_{pp}$, $-2.0\ L_{pp} \leq z \leq 1.0\ L_{pp}$. The brash ice was arranged by injector. The calculation domain of brash ice channel is shown in Figure 3.

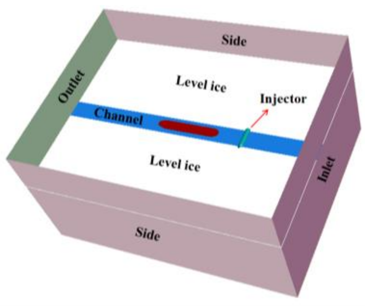

Fig. 3 The computational domain setting of brash ice channel

The overall mesh of the computational domain is shown in Figure 4 (a). The boundary layer mesh adopted a prism layer mesh, and the volume mesh adopted the trimmed mesh. Meshes were refined on the hull surface, the bow and stern, and the free surface. To ensure reasonable simulation of the motion of brash ice in water and the ship-ice contact load, the hull surface mesh and free surface mesh of the ship-ice contact area were further refined, and the mesh of the brash ice movement region was smaller than the size of the brash ice, as shown in Figure 4(b). Since the ship speed was very low, Fr number is only 0.0557. Therefore, to ensure the uniform transition of the boundary layer mesh to the body mesh, the value of wall Y+ of the hull surface below the waterline was less than 1. The wall Y+ of the hull surface is shown in Figure 5.

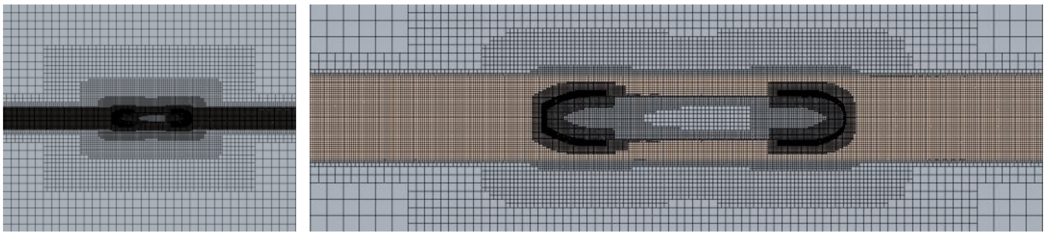

(a) Overall mesh (b) Refined mesh of fore, aft and free surface

Fig. 4 Computational domain mesh

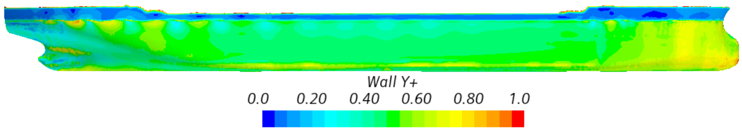

Fig. 5 Y+ of the hull surface

3.3 DEM model of brash ice

The DEM brash ice particle model is the main factor affecting the brash ice resistance. References available mainly used the method of compounding brash ice particles to make brash ice models, and in this way, a combination of multiple basic spherical particles was used for a given geometric shape [21]. The brash ice obtained by this method has two disadvantages: 1) The volume of combined brash ice does not match the actual, so the mass of combined brash ice is smaller than that of brash ice of the same size, and the resistance to the hull is also small. 2) Each combined brash ice consists of multiple or even dozens of spherical particles, resulting in a large number of DEM particles, and the calculation efficiency is reduced. Therefore, the straight brash ice geometry was adopted in this paper, which could simulate the brash ice shape relatively realistically, and reduce the number of DEM particles to improve the computational efficiency. The shape and size of the brash ice model were determined according to the brash ice distribution image of the HSVA ice tank test (as shown in Figures 6a and 6b), the arrangement of the brash ice channel is shown in Figure 6(c).

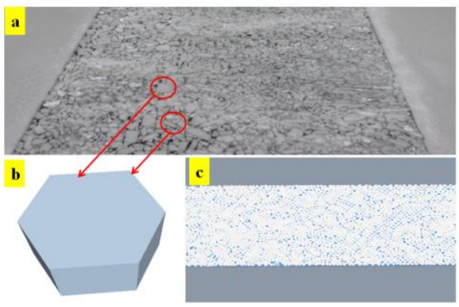

Fig. 6 The shape of the brash ice model and the arrangement of the brash ice channel: (a) Brash ice distribution image of the HSVA ice tank test; (b) Hexagonal brash ice model; (c) The channel arranged by hexagonal brash ice

In order to ensure that the numerical simulation was consistent with the ice tank test, the characteristic parameters of the brash ice model were set according to the data in the Hamburg ice tank test. The characteristic parameters of the model scale brash ice are shown in Table 2. The length of brash ice models is set to about 50 mm, and the corresponding length of full-scale brash ice is about 1.5m. But the actual length of brash ice is slightly different due to the influence of the injector.

Table 2 Characteristic parameters of brash ice

Parameters	Value
Elastic Modulus E (Mpa)	290
Poisson's ratio γ	0.3
Ice-ship friction coefficient f	0.1
Density ρ_i(kg/m^3)	917
Length of brash ice (mm)	about50

4. Numerical simulation validation

The brash ice with different thicknesses were simulated and verified by experimental results in this section. The thickness of brash ice was 39.8mm and 46.3mm, respectively, and the speed of the brash ice was 0.464m/s.

4.1 Analysis of brash ice movement

Figure 7 shows the comparison between the simulation results and the ice tank test when the thickness of the brash ice model is 46.3 mm. When the ship model goes through the brash ice channel, the brash ice will be evacuated to both sides along with the bow of the ship (Fig. 7a), leading to the accumulation of brash ice on both sides of the ship, and then push on the sides of the ship. It is the main reason for friction resistance between the ship and ice. The track of the brash ice among the stern is slightly closed after the ship passes through the brash ice channel (Fig. 7b). The reason for this phenomenon is that the strength of the ice model using the similarity criterion is much smaller than that of the physical ice in the test, resulting in certain plasticity of the brash ice. The brash ice is pushed on both sides of the ship and plastic deformation occurs, so the brash ice in the stern track does not spread out due to the contact force between each other, and the stern track is slightly closed. In the numerical simulation, the brash ice is a polygonal solid, which will not be fracture or deformation, but will be pushed below the ice surface and on the ice surface due to mutual extrusion when it is dislodged from the bow to both sides. (Fig. 7c), but the effect of closing the ice channel in the stern of the ship is more obvious. Although the numerical simulation phenomenon and the ice tank test phenomenon are slightly different because of the different composition and performance, the overall phenomenon is in good agreement.

The accumulation phenomenon of the brash ice on the bow is shown in Figure 8. Due to the influence of the bulbous bow and the large floating angle of the bow, the brash ice cannot slide downward along the hull and can only be discharged to both sides. In the process of displacement, it will accumulate in the bow and the shoulder of the bow. When the thickness of the brash ice increases from 39.8 mm to 46.3 mm, the brash ice is more difficult to be discharged to both sides, resulting in more serious accumulation phenomenon, and even the brash ice is squeezed onto or under the ice surface.

(a) The brash ice dislodged to the sides on the bow　　(b) The stern track of brash ice

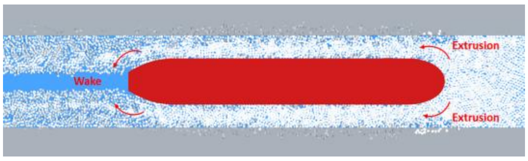

(c) Top view of simulation of brash ice motion

Fig. 7 Comparison between numerical simulation and ice tank test when h_i=46.3 mm

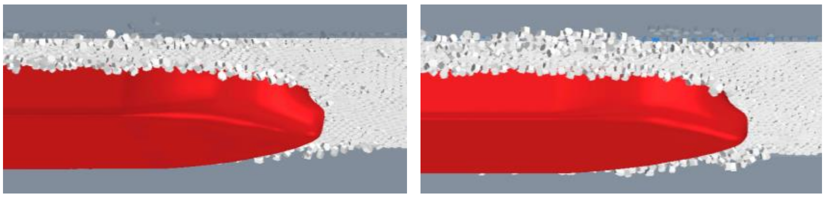

(a) h_i=39.8 mm (b) h_i=46.3 mm

Fig. 8 The accumulation of brash ice on the bow

4.2 Analysis of resistance results

Figure 9 shows the resistance-time curves of the ship in a brash ice channel when the ice thicknesses are h_i=39.8 mm and h_i=46.3 mm, where WaterRes is the water resistance, IceRes$X$ is the longitudinal brash ice resistance, and TotalRes$X$ is the total longitudinal resistance. The brash ice resistance components and the comparison with the test results are shown in Table 3.

As shown in Figure 9, the hull began to contact the brash ice at time of 25s, and the resistance of the brash ice began to gradually increase. With the randomness of ship-ice collisions and friction, the resistance of brash ice also fluctuates.

As shown in Table 3, the ice thickness increases from 39.8 mm to 46.3 mm, but the water-resistance remains almost unchanged, and the brash ice resistance increases from 19.18N to 30.01N, resulting in a decrease in the ratio of water resistance to the total resistance from 27.4% to 19.3 %. The difference between the simulation results and the ice tank test results under the two ice thickness conditions is within 5%, indicating that the simulation results have good accuracy.

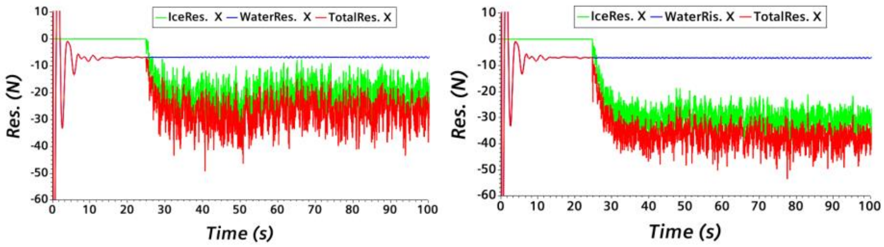

(a) h_i=39.8 mm (b) h_i=46.3 mm

Fig. 9 Time histories of resistance

Table 3 Brash ice resistance components and the comparison with the test results

Ice thickness h_i/mm			Resistance value /N	Percentage (%)	Error (%)
39.8	Experimental result (N)	Total resistance	25.58	----	----
	Simulation result (N)	Water resistance	7.23	27.4	----
		Brash ice resistance	19.19	72.6	----
		Total resistance	26.42	100	+3.28
46.3	Experimental result(N)	Total resistance	36.35	----	----
	Simulation result (N)	Water resistance	7.17	19.3	----
		Brash ice resistance	30.01	80.7	----
		Total resistance	37.18	100	+2.28

5. Conclusions

In this paper, a numerical simulation study of the resistance of the brash ice channel was investigated with the coupling method of CFD and DEM. The influence of grid independence was analyzed. And then the simulation results were compared with the experimental results. It can be concluded that:

(1) The difference between numerical simulation results and experimental results is within 6% with the increase of the grid number. So the numerical simulation results are not affected by the number of grids.

(2) The phenomenon of brash ice movement in the channel was in good agreement with the test results. The brash ice was dislodged from the bow to the sides of the ship, and the accumulation of the brash ice on the bow, the stern track of the brash ice, and the contact force between the hull and the brash ice could be captured.

(3) The precision of numerical simulation was high. As the ice thickness is 39.8 mm and 46.3 mm, the difference between the total resistance of the brash ice channel and the experimental results was 3.28% and 2.28% respectively, and both of the errors were within 5%. Brash ice resistance accounted for more than 70% of the total resistance of the brash ice channel. The proportion of the brash ice resistance increased with the ice thickness increasing.

References

Cho S-R, Jeong S-Y, Lee S. Development of effective model test in pack ice conditions of square-type ice model basin[J]. Ocean engineering, 2013, 67: 35-44.

Cundall P A, Strack O D. A discrete numerical model for granular assemblies[J]. geotechnique, 1979, 29(1): 47-65.

Dobrodeev A, Sazonov K. Ice resistance calculation method for a ship sailing via brash ice channel[C]. Proc., 25th Int. Conf. on Port and Ocean Engineering under Arctic Conditions, 2019: 1-12.

Guo C-Y, Xie C, Zhang J-Z, et al. Experimental investigation of the resistance performance and heave and pitch motions of ice-going container ship under pack ice conditions[J]. China Ocean Engineering, 2018, 32(2): 169-178.

Guo C-Y, Zhang Z-T, Tian T-P, et al. Numerical simulation on the resistance performance of ice-going container ship under brash ice conditions[J]. China Ocean Engineering, 2018, 32(5): 546-556.

Guo W, Zhao Q-S, Tian Y-K, et al. Research on total resistance of ice-going ship for different floe ice distributions based on virtual mass method[J]. International Journal of Naval Architecture and Ocean Engineering, 2020, 12: 957-966.

Haider A, Levenspiel O. Drag coefficient and terminal velocity of spherical and nonspherical particles[J]. Powder technology, 1989, 58(1): 63-70.

Huang L, Tuhkuri J, Igrec B, et al. Ship resistance when operating in floating ice floes: A combined CFD&DEM approach[J]. Marine Structures, 2020, 74: 102817.

Jeong S-Y, Jang J, Kang K-J, et al. Implementation of ship performance test in brash ice channel[J]. Ocean Engineering, 2017, 140: 57-65.

Jeong S-Y, Kim H-S. Study of ship resistance characteristics in pack ice fields[C]. Proceedings of the 25th International Conference on Port and Ocean Engineerin g under Arctic Conditions. Delft, Netherlands, June, 2019: 9-13.

Ji S, Li Z, Li C, et al. Discrete element modeling of ice loads on ship hulls in broken ice fields[J]. Acta oceanologicasinica, 2013, 32(11): 50-58.

Karulina M M, Karulin E B, Tarovik O V. Extension of FSICR method for calculation of ship resistance in brash ice channel[C]. Proceedings of the 25th International Conference on Port and Ocean Engineering under Arctic Conditions June, 2019: 9-13.

Kim J-H, Kim Y, Kim H-S, et al. Numerical simulation of ice impacts on ship hulls in broken ice fields[J]. Ocean Engineering, 2019, 182: 211-221.

Kim M-C, Lee S-K, Lee W-J, et al. Numerical and experimental investigation of the resistance performance of an icebreaking cargo vessel in pack ice conditions[J]. International Journal of Naval Architecture and Ocean Engineering, 2013, 5(1): 116-131.

Kim M-C, Lee W-J, Shin Y-J. Comparative study on the resistance performance of an icebreaking cargo vessel according to the variation of waterline angles in pack ice conditions[J]. International Journal of Naval Architecture and Ocean Engineering, 2014, 6(4): 876-893.

Luo W, Jiang D, Wu T, et al. Numerical simulation of an ice-strengthened bulk carrier in brash ice channel[J]. Ocean Engineering, 2020, 196: 106830.

Luo W-Z, Guo C-Y, Wu T-C, et al. Experimental research on resistance and motion attitude variation of ship–wave–ice interaction in marginal ice zones[J]. Marine Structures, 2018, 58: 399-415.

Menter F R. Two-equation eddy-viscosity turbulence models for engineering applications[J]. AIAA journal, 1994, 32(8): 1598-1605.

Norouzi H R, Zarghami R, Sotudeh-Gharebagh R, et al. Coupled CFD-DEM modeling: formulation, implementation and application to multiphase flows[M]. John Wiley & Sons, 2016.

Polojärvi A, Gong H, Tuhkuri J. Comparison of Full-scale and DEM simulation Data on Ice Loads Due to Floe Fields on a Ship Hull[C]. International Conference on Port and Ocean Engineering under Arctic Conditions, 2021.

Trafi S. Guidelines for the Application the Finnish-Swedish Ice Class Rules: June, 2011.

Trafi. Finnish-Swedish Ice Class Rules 2010: Finnish Transport Safety Agency Espoo, Finland, 2010.

Van Den Berg M, Lubbad R, Løset S. The effect of ice floe shape on the load experienced by vertical-sided structures interacting with a broken ice field[J]. Marine Structures, 2019, 65: 229-248.

Wang C, Hu X, Tian T, et al. Numerical simulation of ice loads on a ship in broken ice fields using an elastic ice model[J]. International Journal of Naval Architecture and Ocean Engineering, 2020, 12: 414-427.

Yang B, Sun Z, Zhang G, et al. Numerical estimation of ship resistance in broken ice and investigation on the effect of floe geometry[J]. Marine Structures, 2021, 75: 102867.

Yang B, Zhang G, Huang Z, et al. Numerical simulation of the ice resistance in pack ice conditions[J]. International Journal of Computational Methods, 2020, 17(01): 1844005.

Zhang J N, Shang Y C, Zhang L. Ice resistance model test technology for 110K tanker adopting FSICR ice class IA[C]. Advanced Materials Research, 2013: 1117-1123.

Zhou L, Ling H, Chen L. Model tests of an icebreaking tanker in broken ice[J]. International Journal of Naval Architecture and Ocean Engineering, 2019, 11(1): 422-434.

Zong Z, Yang B, Sun Z, et al. Experimental study of ship resistance in artificial ice floes[J]. Cold Regions Science and Technology, 2020, 176: 103102.